



Deterministic seismic hazard assessment for the Makkah region, western Saudi Arabia

Hani Mahmoud Zahran¹ · Vladimir Sokolov¹ · Salah El-Hadidy¹

Received: 25 April 2019 / Accepted: 10 July 2019 / Published online: 29 July 2019
© Saudi Society for Geosciences 2019

Abstract

Rapid social and industrial development of the Makkah and Jeddah regions emphasizes necessity of reassessment of seismic hazard, results of which are essential for aseismic design, emergency management, and insurance regulations. In this work, the deterministic seismic hazard studies are applied to evaluate level of seismic hazard for the Makkah region using the up-to-date geophysical, geological, and seismological database, and using different techniques. The assessment has been performed in terms of peak ground acceleration (PGA) and presumably active faults are considered as sources of earthquakes. Results of the study show that, in the context of the used models of seismic sources, the level of seismic hazard in the region is controlled by magnitude of earthquakes that may occur at the intersection of NE-SW faults (the Ad Damm fault zone and the Wadi Fatima Shear Zone) and the NNW-oriented faults that run parallel to the Red Sea coast (Red Sea Margin Faults group). It is important to make accurate mapping of faults using up-to-date data and to estimate if the faults are active at present. Particular attention should be given to careful estimation of maximum magnitude of possible earthquakes that can occur along the active fault.

Keywords Seismic hazard · Makkah region · Saudi Arabia

Introduction

Spreading of the Red Sea and volcanism are the sources of seismicity in the western Saudi Arabia (e.g., El-Isa and Al Shanti 1989; Al-Amri 1995; Al-Saud 2008; Bosworth 2015; El-Hadidy 2015, see also Zahran et al. 2016, for review). Historical data show evidences of large earthquakes that may happen in the area (e.g., Poirier and Taher 1980; Ambraseys and Adams 1988; Ambraseys and Melville 1988). One of the largest events in the region (magnitude M_S 6.5, 11 January 1941, epicentral intensity MSK VIII) occurred near the current Saudi Arabia–Yemen border (Ambraseys et al. 1994). Recently (January 23, 2014), several earthquakes (magnitude of the largest event M_L 5.1) happened about 50 km northeast of Jizan city (El-Hadidy 2015; El-Hadidy et al. 2015).

Volcanic activity in the region during last 30 million years resulted in lava fields (harrats) in western Saudi Arabia (e.g., Camp and Roobol 1989, 1992; Camp et al. 1991; Downs et al. 2018). As noted by Zahran and El-Hady (2017) and Downs et al. (2018), more than 20 within-plate volcanic eruptions had occurred in the Arabian Peninsula during the past 1500 years and may occur in the future in the western region of Saudi Arabia. The latest eruption occurred near the Al-Madinah city, northern part of Harrat Rahat, in 1256 CE; the eruption was accompanied by a series of earthquakes (e.g., Camp et al. 1987; Moufti et al. 2013; El-Masry et al. 2013). The 2009 earthquake swarm occurred in Harrat Lunayyir (magnitude of the largest event M_L 5.4) may be also considered as the result of volcanic activity, namely by magmatic dike intrusion, as shown by geologic, geodetic, and seismic data (Abdelfattah et al. 2016; Baer and Hamiel 2010; Duncan and Al-Amri 2013; Mukhopadhyay et al. 2013; Pallister et al. 2010).

Two famous sites of the Muslim world, the holy cities of Makkah Al-Mukarramah and Al-Madinah Al-Munawarah, are located in western Saudi Arabia and nearly 6.7 million people are living in the Makkah-Jeddah-Madinah regions. The population is increasing by several millions every year during the Hajj. The circumstance together with the rapid industrial and social development of these regions emphasizes

Handling editor: Abdullah M. Al-Amri

✉ Vladimir Sokolov
sokolov.v@sgs.org.sa

¹ National Center for Earthquakes and Volcanoes, Saudi Geological Survey, Jeddah, Saudi Arabia

necessity of reassessment of seismic hazard based on the up-to-date geophysical, geological, and seismological database. Results of the reassessment provide essential parts of building codes development, emergency and land-use planning, and insurance applications.

Studies of seismic hazard for the Makkah region were performed by several researchers, which applied mostly probabilistic approach and considered areal seismic source zones. The earthquake catalog collected during only recent few decades was analyzed in these studies; the shortage of the data that may lead to high level of uncertainty in estimations of characteristics of seismicity (e.g., earthquake recurrence and shape of areal seismic source zones) considered in probabilistic assessment. In this work, we used modified deterministic approaches that do not require utilization of earthquake recurrence parameters. The assessment of seismic hazard is based on consideration of active faults delineated using recent geological, seismological, and aeromagnetic data.

Input data

Tectonics

The Arabian Plate (Fig. 1) that is one of the youngest lithosphere plates is surrounded by relatively active tectonic zones, namely the Gulf of Aden, the Red Sea, the Gulf of Aqaba and the Dead Sea transform zone, and the Taurus and the Zagros Mountains (e.g., Girdler 1991; Johnson 1998; Stern and Johnson 2010). The western part of the Arabian Plate is called as the Arabian Shield—a stable craton, where Precambrian rocks are exposed due to Mesozoic and Cenozoic uplift. The Shield is separated from the Red Sea by a relatively narrow coastal plain of Cenozoic sediments.

As noted by many researchers (e.g., Pallister 1986; Camp and Roobol 1992; Bosworth 2015; Roobol and Kadi 2008; Roobol and Stewart 2009; see also Zahran et al. 2016), a belt of NNW-oriented faults (so-called Red Sea Margin Fault Belt, RSMF) is located in the Arabian Shield within about 100 km of the Red Sea eastern coast. The belt contains many dikes that run parallel the coast along its entire length. Magnetic data clearly reveal the dikes, which are usually 200–300 m thick and nearly vertical. Roobol and Kadi (2008, 2014) demonstrated that the belt contains two fault systems of different ages. The oldest is the Foothills Fault System with age 24 ± 2 Ma in the northern part and between 30 and 27 Ma in the southern part. The faults divide the Precambrian rocks into horst-graben structures. The younger system of faults was named as the Red Sea Coast Plain Fault system. The faults cut the Foothills faults and they lie beneath the gravels of the coastal plain; the faults can be traced along the entire length of the Red Sea.

Another distinctive feature of the western Saudi Arabia is a system of NE-SW oriented transform faults that offset the Red Sea median trough and cross the submarine platforms (e.g., Whiteman 1976; Blank 1977; Pallister 1986; El-Isa and Al Shanti 1989; Moore and Al-Rehaili 1989; Roobol and Kadi 2014). Some of the faults come ashore in Saudi Arabia and may displace upper Cenozoic structures. As noted by Thenhaus et al. (1989) and El-Isa and Al Shanti (1989), the recent inland seismic activity, as well as some historical earthquakes (Poirier and Taher 1980), may be related to the faults.

Zahran et al. (2016) selected the area in the central part of the RSMF belt as a separate seismic source zone (so-called Jeddah-Makkah zone) because of relatively dense spacing of NE-SW lineaments. Aeromagnetic data indicate tens of lineaments (e.g., Zahran et al. 2003), the half of which are visible as linear valleys (or wadis in Arabic language) on the Google Earth images. The others are hidden beneath coastal gravel fans but they can be detected from aeromagnetic data. As it is evident from the data, some of the NE-SW lineaments do overlap the NNW dikes of the Red Sea Margin Fault Belt. One of the most prominent NE-trending structure in the region is the Ad Damm fault that extend more than 100–130 km inland (e.g., El-Isa and Al Shanti 1989). The fault lies between the Asir and Jiddah tectonic terranes (e.g., Stern and Johnson 2010). As noted by Pallister (1986) and El-Isa and Al Shanti (1989), the Ad Damm fault reveals Precambrian right-lateral movement, as well as younger movement. The fault is associated with earthquake activity (e.g., Merghelani et al. 1981; see also next section of this paper).

The studied area (Makkah region) lies between the Ad Damm fault to the south, and the NE-oriented Wadi Fatima Shear Zone, which passes the western part of the Jiddah terrane, to the north (Fig. 1) (see also Pallister 1986; Moore and Al-Rehaili 1989; Kassem and Hamimi 2018). Al-Saud (2008) provided description of the fault system and structural zones in region summarizing information from several studies, and classified earthquakes occurred in the vicinity of the Ad Damm fault zone and in the Wadi Fatima Shear Zone as tectonic seismic activity along subsurface active faults.

Seismicity (historical and instrumental)

Historically, seismic activity in the Arabian shield appears to be low. Most of the moderate and strong earthquakes are located along the axis of Red Sea southwest of the Jeddah city (Fig. 1). Historical data (see, for example, short review by El-Isa and Al Shanti 1989; Osman 2012) indicated several earthquakes that occurred in the region around Makkah. The strongest earthquake occurred in 1121 AD; the earthquake damaged the Yemeni (southern) corner of the Ka'ba in Mecca and destroyed part of the mosque of the Prophet in Al-Medina. It seems that earthquake might be occurred in

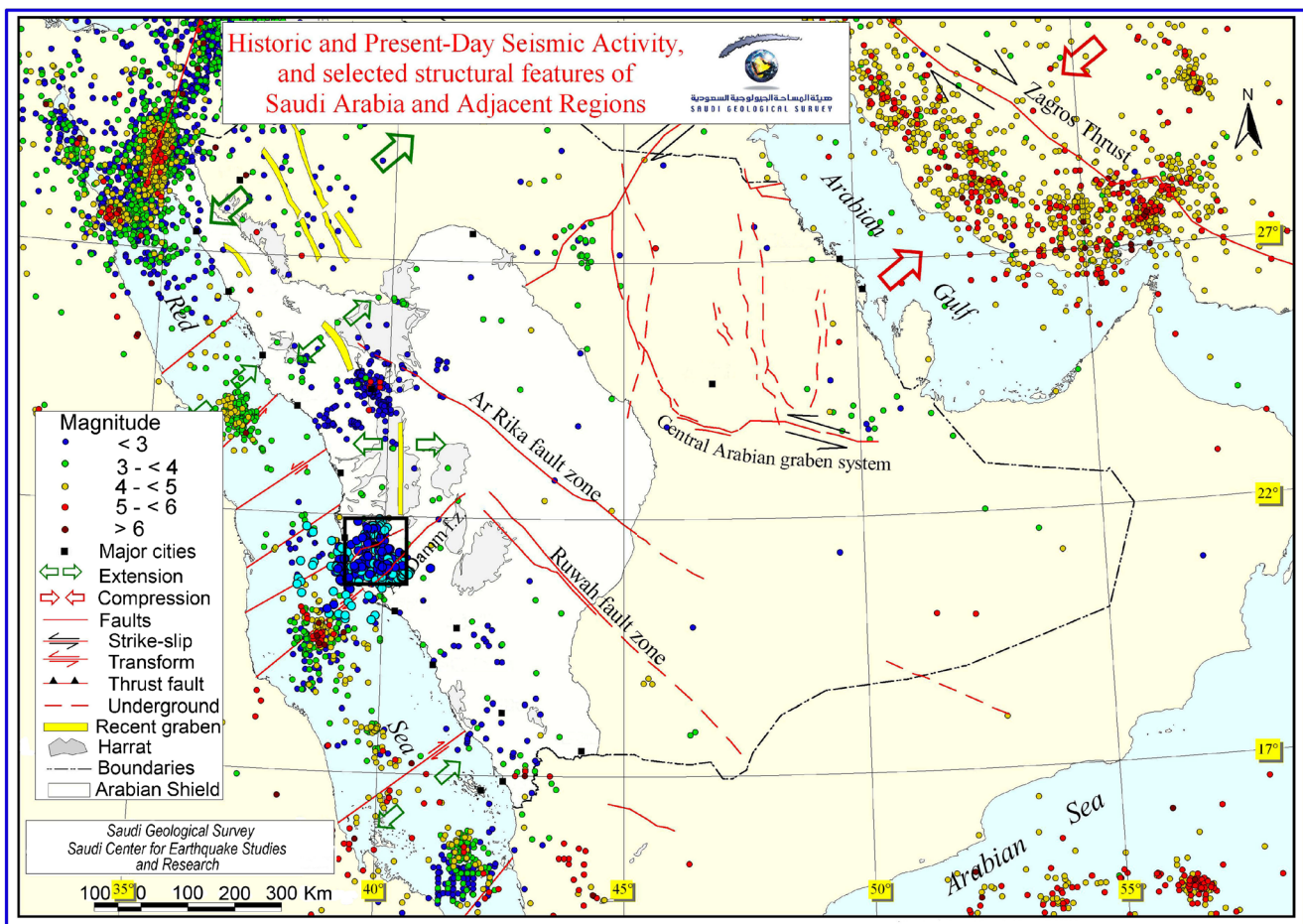


Fig. 1 Historical and recent seismicity (up to 1995) and structural elements in and around Saudi Arabia (after Saudi Geological Survey). Black rectangle show the study area

the Red Sea. Strong shaking was occurred in Mecca in 1408 AD; an arch at the sacred mound of Al-Marwa, 200 yards north of the Ka'ba, was destroyed. An earthquake that probably occurred along the Ad Damm fault in 1269 AD was felt at Taif.

Figure 2 shows distribution of epicenters of earthquakes since 1980. There are several areas of increased seismic activity. Among earthquakes occurred around the city of Makkah and recorded after installation of Saudi National Seismic Network (Endo et al. 2007), the following events should be mentioned (see Fig. 3): M_L 4.1 earthquake (3 October 1993) accompanying by a set of aftershocks with M_L up to 3.4; M_L 4.1 earthquake (18 June 1994); M_L 3.7 earthquake (12 September 2005). Recently, the Al Markh Valley area, which lies at a distance about 60 km southeast of the city of Makkah, was shocked by earthquake swarm (16 events with magnitudes M_L from 0.8 to 2.2) during the period from 5 to 10 January 2019. The earthquake swarm continued for a few months producing about 50 earthquakes (depth less than 4 km) with maximum magnitude M_L 2.8. Despite small magnitudes, these earthquakes were felt inside and around the epicentral area.

Aeromagnetic data

As can be seen from Fig. 3, epicenters of earthquakes recorded since 1993 are stretched along linear zones. It has been shown recently (Zahran et al. 2017) that analysis of aeromagnetic data may be used for accurate mapping of geological structures covered by sediments in the western Saudi Arabia. Therefore, the existing aeromagnetic data were re-analyzed to gain a better understanding of location of lineaments in the Makkah region. The analyzed data cover an area with dimensions 274 km (N-S) by 173 km (E-W). The data includes part of a large regional survey carried out in 1965 along lines at 800 m spacing. The data were leveled and merged into a single grid in 2001, as a part of the regional compilation made by Saudi Geological Survey (SGS) for the data collected aeromagnetic surveys for the Arabian Shield, central Red Sea, and Phanerozoic rock outcrops (Zahran et al. 2003).

The procedure of calculation and analysis of directional tilt derivative (DTD) described by Stewart and Miller (2018) was used in the new analysis. As noted by the authors, the tilt derivative is of the most useful method that can be used to analysis of potential field data to detect linear trends in the data

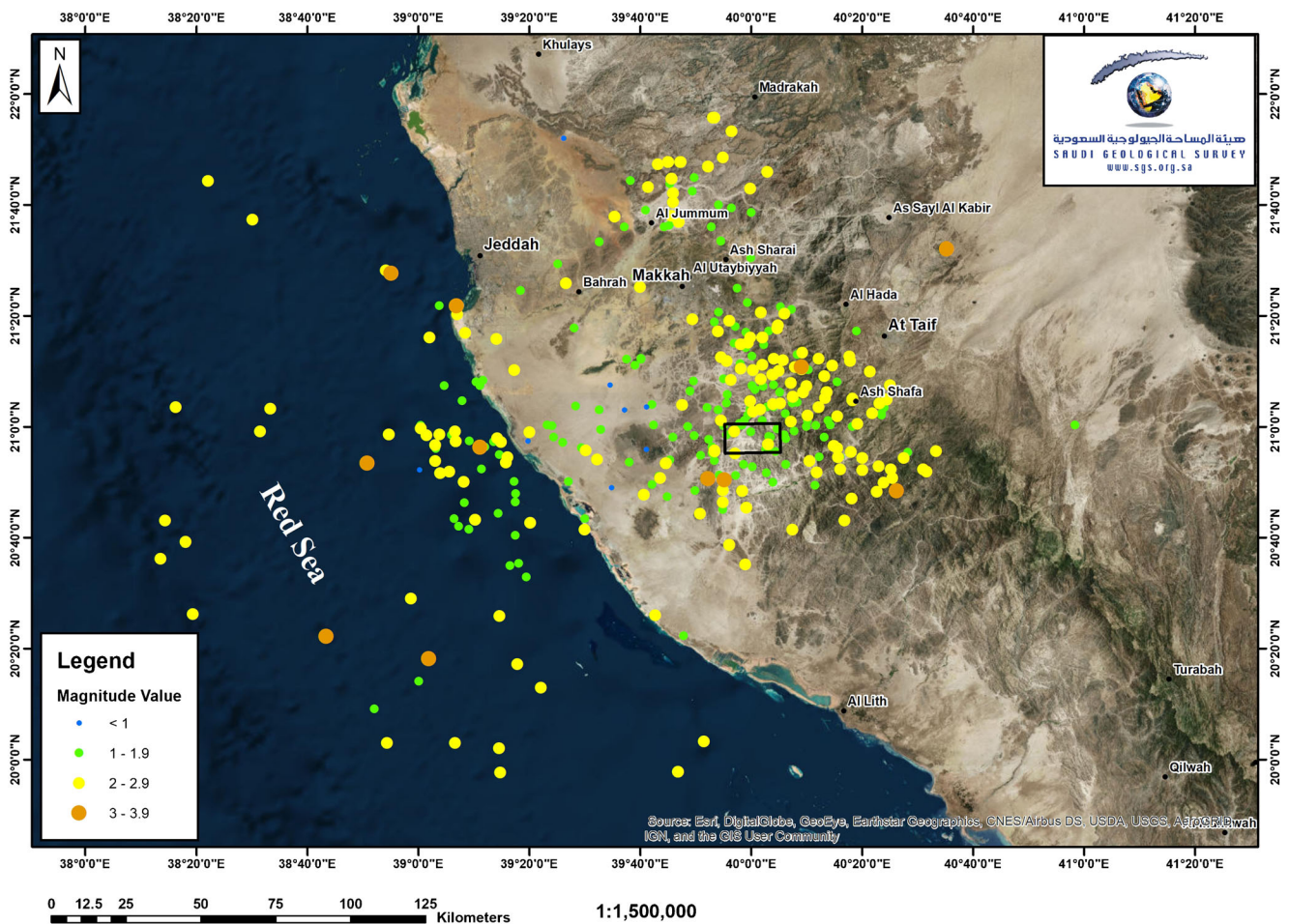


Fig. 2 Seismicity in and around Makkah region since 1980 (based on data collected by SGS, KSU, and Merghelani et al. 1981). Black rectangle shows location of the 2019 swarm (see text and Fig. 3)

and to reveal low-amplitude features. Figure 4 shows the DTD images composed for the studied region.

Analysis of aeromagnetic data for Makkah region shows that the epicenters of earthquakes occurred in the region since 1993 are stretched along the NE-SW trending faults. Location of the largest recorded events is controlled by intersection of the NE-SW faults (e.g., Makkah Shear Zone, Ad Damm fault) and the NNW-oriented faults that run parallel to the Red Sea coast (RSMF group of faults). Results of the analysis, together with results of the seismotectonic and geological studies for the region described above, are used in our work for construction of model of active faults for deterministic seismic hazard assessment.

Seismic hazard assessment

Methodology

Seismic hazard assessment (SHA) for the region was performed by several researchers from different points of view.

Most studies related to the SHA for western Saudi Arabia (e.g., Deif et al. 2009; Babiker et al. 2015; Zahran et al. 2015; Rehman et al. 2016, 2017; Zahran et al. 2016) included the Makkah region into relatively large areal seismic source zones delineated by consideration of the geological and tectonic settings, as well as the information on historical and instrumental seismicity.

Al-Saud (2008) provided thorough discussion of tectonic features and seismicity of the areas around Jeddah and Makkah and selected two local areal seismic source zones, namely Ad Damm fault zone (NE-SW trending zone along the Ad Damm fault with relatively high level of recorded seismicity) and the Nu'man-Makkah-Fatima zone (NNW trending zone that includes densely located NE-SW and the NNW faults with moderate seismic activity attributed to Red Sea rifting). Osman (2012) estimated seismic hazard for the holy city of Makkah using probabilistic and deterministic approaches considering two inland areal seismic source zones. Fnais et al. (2014) used seismological, geological, and geophysical data and delineated several seismic source zones in the region, namely three zones along the central part

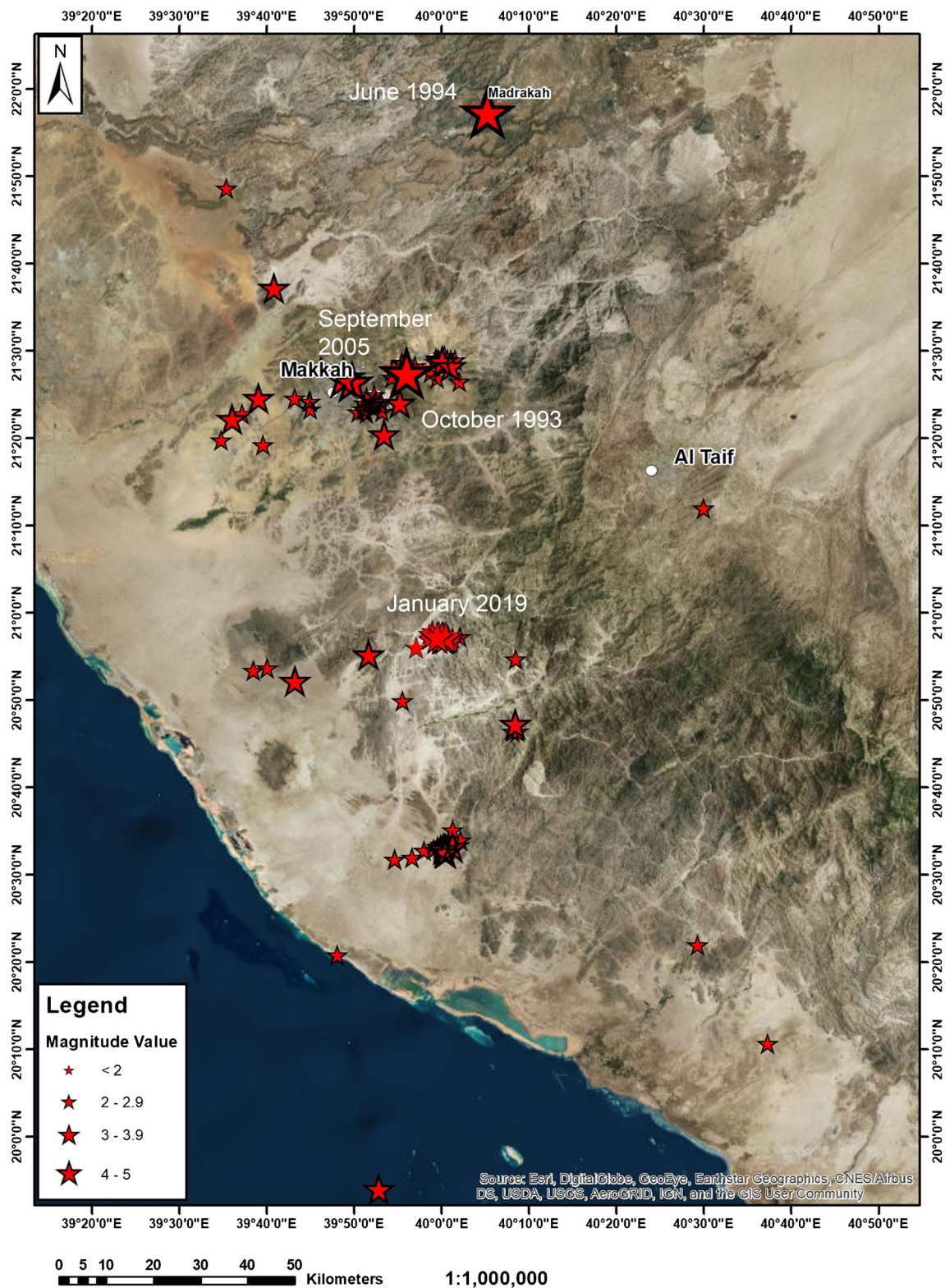


Fig. 3 Epicenters of earthquakes recorded in the study area since 1993

of the Red Sea and two inland zones. The inland zones were selected considering main tectonic faults, location of earthquakes, and characteristics of seismicity. The so-called Jeddah-Makkah seismic source zone delineated by Fnais

et al. (2014) extends NE from the Red Sea coast and includes the Wadi Fatima fault zone and Ad Damm fault zone. Thus, all modern studies consider several areal inland sources, the size and shape of which are delineated differently.

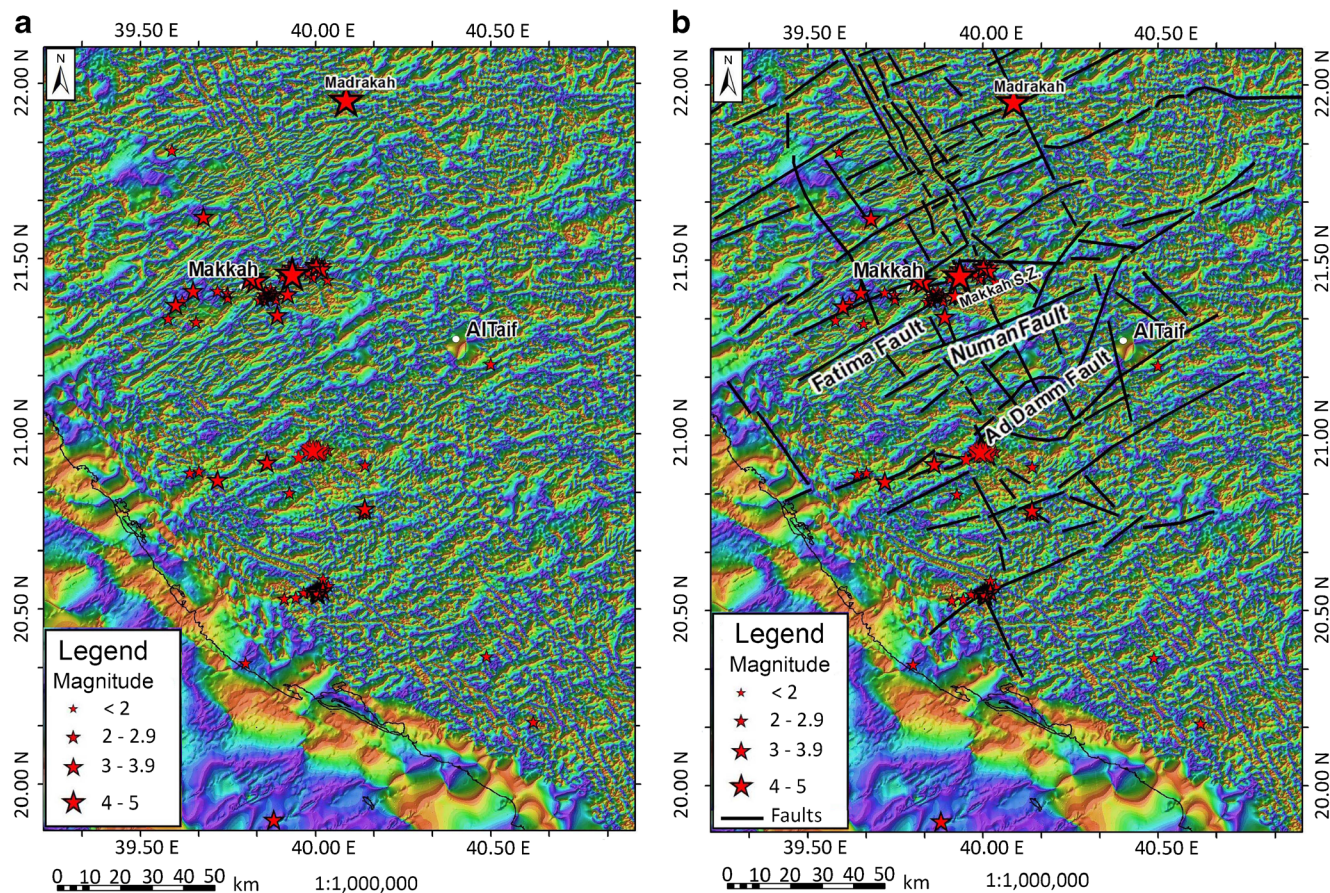


Fig. 4 Aeromagnetic data, directional tilt derivative (DTD) calculated for the region of study. **a** The data used for analysis and detection of linear trends. **b** The data shown together with lineations obtained from geology

maps (Fatimah fault; Makkah Shear Zone, Numan fault and Ad Damm fault) and the lineations revealed from DTD analysis

Estimations of characteristics of seismicity (e.g., parameters of recurrence relationship) and delineation of the areal seismic source zones were performed in the abovementioned studies using earthquake catalog collected during recent few decades. Obviously, the limited database lead to high level of uncertainty in estimations of parameters of recurrence relationship and in shape of seismic source zones.

Deterministic approach to estimations of seismic hazard (DSHA) does not consider earthquake recurrence. The traditional DSHA uses a limited set of earthquake scenarios (the maximum expected magnitude earthquake occurred at the smallest distances from the site of interest) based on variations of parameters of surrounding seismogenic zones (e.g., Klügel et al. 2006). However, there is always a high level of uncertainty related to (a) determination of the maximum expected magnitude of future earthquake and to (b) the level of ground motion. Thus, it is necessary to identify a “reasonably large” event and some reasonable level of ground motion associated with this event bearing in mind that the larger earthquakes (and larger ground motion intensity) may also occur. Such event is historically called as a “Maximum Credible Earthquake,” or MCE, or as a “Maximum Considered

Earthquake.” When ground motion prediction equations (GMPE) are applied to estimate level of ground motion (GM), then a specified ground motion probability level (the number of standard deviations σ , sigma, from the median ground motion level, typically either 0 or 1 sigma) is used. Thus, in DSHA, the resulting ground motion is not a “worst-case” but a “reasonably worst case” ground motion, and the result may be very sensitive to the scenario magnitude and to the chosen ground motion probability level. DSHA is frequently used for analysis of consequences of single earthquake (e.g., emergency response and recovery, special design of critical infrastructures) in the case of well-known active faults (McGuire 2001).

Neo-deterministic method for estimation of seismic hazard (NDSHA, see Zuccolo et al. 2011, and Panza et al. 2013, 2014, for a review) implies numerical modeling of the processes of rupture in seismic sources and propagation of seismic waves. Synthetic seismograms are computed for several scenario earthquakes (MCEs) assigned to seismic source zones. A set of estimations of ground motion displacement amplitudes is produced at the site of interest and the maximum value from the set is selected as characteristic of seismic

hazard. The NDSHA method has been applied worldwide (e.g., Panza et al. 2013, 2014; Panza 2017) for seismic hazard assessment of different scales and purposes.

Magnitudes of maximum credible earthquakes (MCM) are estimated using the data from different sources and, in most cases, the estimations are characterized by considerable uncertainty. Sokolov (2017) discussed limitations of the NDSHA method and suggested using stochastic generation of distribution of maximum credible earthquakes inside seismic source zone together with application of ground motion prediction equations (GMPEs). Ground motion is estimated using the GMPEs as the median value of ground motion for given magnitude and distance plus randomly generated variation representing inherent uncertainty of ground motion. The MCM values are also considered as random variables. Consequently, seismic hazard for every site is described not by a single ground motion value (e.g., the maximum of the estimations from all considered earthquakes), but by a probability density function and a cumulative distribution function for considered ground motion parameter. It brings up the question, what probability of exceedance should be used to determine the desired value of ground motion from the cumulative distribution function, and some suggestions related to the problem were provided by Sokolov (2017).

In our study, for deterministic seismic hazard analysis based on maximum credible earthquakes, two models of seismic source zones and correspondingly two approaches for the analysis are used. In the first model, the active faults located in the studied area are treated as linear source zones (Fig. 6a). It is assumed that the MCE events may occur at any point along the faults. Two variants of distribution of the maximum magnitude values along the faults are considered. The first variant implies that the MCM earthquakes can occur wherever it is possible, i.e., at all points along the faults. Hereafter, the variant is called as LS_AP (linear source, all points) model. In the second variant, the earthquakes with maximum magnitude may occur only in the vicinity of intersection of two faults that belong to the major fault systems, i.e., the NNW-oriented faults and the NE-SW trending faults. The variant is called as LS_IF (linear source, intersection of faults) model. To determine the value of magnitude M_i for any earthquake that may occur along fault, first, we define an area around the intersection (e.g., by radius R_a), within which the magnitude M_i is accepted to be equal to maximum magnitude M_{MAX} . Then, the magnitude M_i is determined depending on the distance R_i between epicenter of the i -earthquake and the nearest intersection as follows:

$$\begin{aligned}
 M_i &= M_{MAX}, \text{ for } R_i \leq R_a \\
 M_i &= M_{MAX} - (1 - \Delta m \times \exp(-R_{eff}/d)), \text{ for } R_i > R_a
 \end{aligned}
 \tag{1}$$

where Δm is the difference between the magnitude of

maximum credible earthquake M_{MAX} assigned to the intersection and the magnitude of earthquake M_{MIN} that may occur at sufficiently large distance from the intersection, that is $\Delta m = M_{MAX} - M_{MIN}$; R_{eff} is the “effective distance” determined as the actual distance between the epicenter of i -earthquake and the intersection R_i minus radius of area around the point of intersection R_a , within which the magnitude is accepted to be equal to M_{MAX} , i.e., $R_{eff} = R_i - R_a$; d is the diminution parameter. Figure 5 illustrates, as example, application of Eq. 1 for estimation of magnitudes of earthquakes that can occur along hypothetical fault with one intersection.

When using the linear source model, several MCE scenario events are generated covering the entire length of every fault. The dimensions of the earthquake sources are estimated via magnitude-dimension relations provided by Vakov (1996). The depth of all earthquakes (center of the fault plane) is accepted to be equal to 7.0 km. The orientation of the earthquake sources (strike angle) coincides with orientation of the corresponding fault, and the dip angles are fixed as 89° (almost vertical fault). Figure 6a shows linear source model of presumably active faults.

The second model of earthquake sources used in our study coincides with the approach proposed by Sokolov (2017). The active faults are considered as narrow areal zones with a width about 6 km; therefore, the model is called as the AZ (areal zones) model (Fig. 6b). A set of MCE scenario events are generated to cover the entire area of every zone; dimensions and orientation of every earthquake source are assigned as that in the LS model. Magnitude of every earthquake is estimated as $M_{MAX} - \Delta M$, where ΔM is the random value with uniform distribution between 0.0 and 0.25 units of magnitude. Depth of every scenario earthquake is assigned as the random value with uniform distribution between 5 and 25 km. The ground motion values are calculated using selected GMPEs considering random variations of ground motion. Thus, the AZ model implicitly takes into account uncertainties in the location and

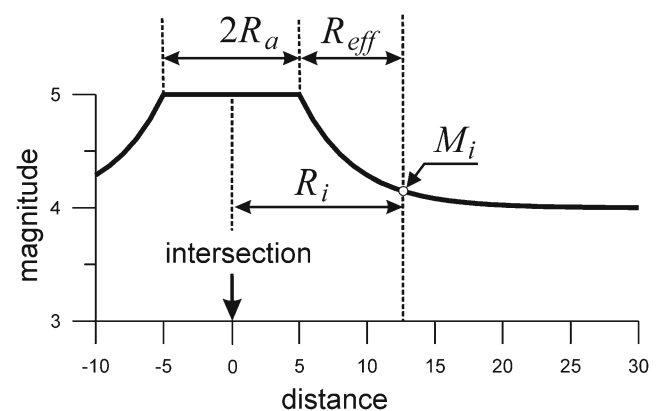
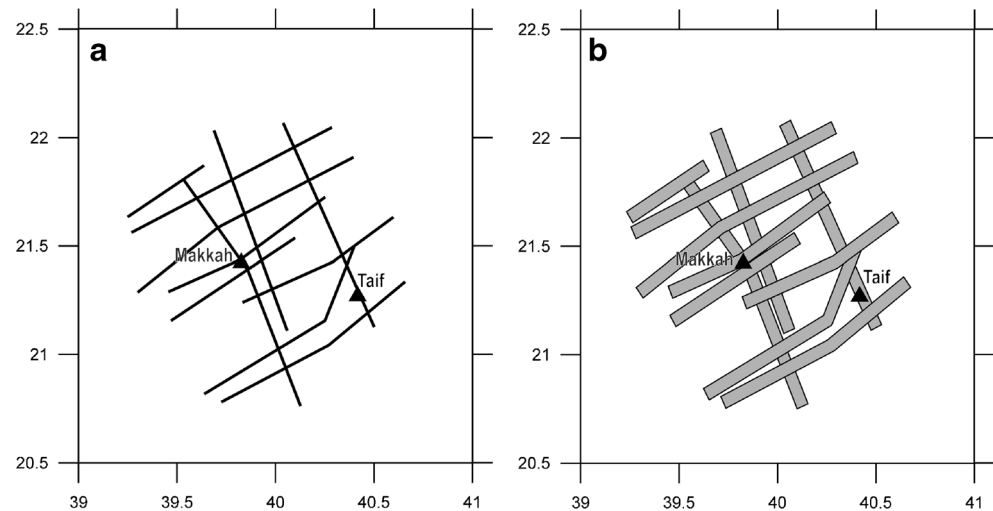


Fig. 5 Example of distribution of magnitudes of earthquakes that can occur along hypothetical fault with one intersection. Magnitudes are estimated using Eq. 1 with the following parameters: $M_{MAX} = 5.0$; $M_{MIN} = 4.0$, $R_a = 5$ km; $d = 4$ km

Fig. 6 Models of earthquake sources used in deterministic seismic hazard estimations. **a** Linear source (LS) model. **b** Narrow areal zones (AZ) model



magnitude of possible earthquakes, as well as the scatter in ground motion parameters.

Distribution of ground motion parameters in both variants is calculated using a set of GMPEs with slightly modified scheme that was accepted in our recent studies related to assessment of seismic hazard in Saudi Arabia (Zahran et al. 2015; Sokolov et al. 2017; Zahran and El-Hady 2017; Sokolov and Zahran 2018). The Atkinson and Boore' model (2006) is used for the stable continental region of Saudi Arabia in conjunction with the equations for active shallow crustal sources, namely the models of Zhao et al. (2006), Boore and Atkinson (2008), Campbell and Bozorgnia (2008), and Akkar et al. (2014). Equal weights (0.2) are assigned for all GMPEs. Normal type of faulting is considered in the equations for the NNW faults and strike-slip type of faulting—for the NE-SW faults. All GMPEs allow taking into consideration local site effects through the average shear-wave velocity of the upper 30-m column (V_{s30}). We perform calculations using $V_{s30} = 800$ cm/s and $V_{s30} = 400$ cm/s that corresponds to site classes B (rock) and C (dense soil) based on classification accepted in Saudi Building code (SBC 301-2007, Chapter 14).

In this study, peak ground acceleration (PGA, geometric mean of two horizontal component) is used as the characteristic of earthquake ground motion. In the LS model, the ground motion values are calculated using the median GMPE and median + 1 standard deviation. Firstly, the PGA values are calculated from every scenario earthquake for the nodes of grid ($0.02^\circ \times 0.02^\circ$). Secondly, the maximum value from a set of calculated PGAs is selected for the further analysis. In this manner, we consider an envelope of estimations from several scenario earthquakes (e.g., Klügel 2008). Similar approach was used by Rehman et al. (2016); however, the work was based on relatively large areal seismic sources. Uncertainties in characteristics of earthquakes (location and size of sources, and magnitude) are accounted by smoothing of the PGA values in the similar way as it is usually done, for example, in the smoothing

seismicity approach. The Gaussian distribution function is used to smooth the PGA values as follows:

$$\hat{a}_i = \frac{\sum_j a_j e^{-\Delta_{i,j}^2/c^2}}{\sum_j e^{-\Delta_{i,j}^2/c^2}} \quad (2)$$

where \hat{a}_i is the smoothed PGA value in the i -th node, a_j is the PGA value in the j -th grid node, c is the parameter of the smoothing function (correlation distance), and $\Delta_{i,j}$ is the distance between the i -th and j -th nodes. The smoothing operator practically does not take into account PGA values located at distances more than $3c$.

The following scheme of calculation of ground motion is applied in the AZ variant (see also Sokolov 2017). Firstly, a random value $\varepsilon_{j,k}$ is generated for every seismic event j and every site location k considering normal distribution. The ground motion residual $\delta_{i,j,k}$ is calculated for every GMPE i using the GMPE-specific standard deviation σ_i as $\delta_{i,j,k} = \varepsilon_{j,k} \times \sigma_i$. Secondly, a set of ground motion parameters $Y_{i,j,k}$ is estimated considering all GMPEs as $\ln Y_{i,j,k} = \overline{\ln Y_{i,j,k}} + \delta_{i,j,k}$, where $\overline{\ln Y_{i,j,k}}$ denotes the median value of ground motion parameter predicted by the i -GMPE for given earthquake j and site location k . Finally, the resulted ground motion value is calculated as a weighted average $\ln Y_{j,k} = (\sum_{i=1}^n \ln Y_{i,j,k} \times w_i) / \sum_{i=1}^n w_i$, where n is the number of GMPEs and w_i is the weight assigned for particular GMPE. The probability density functions (PDF_k) and cumulative distribution functions (CDF_k) are constructed for every considered location k using the data from all earthquakes.

Results

In our work, as the primary value used in all calculations, the maximum magnitude for the MCE events is accepted as

$M_{MAX} = 5.0$; the value is based on the models used in previous studies related to seismic hazard assessment in the region (Osman 2012; Rehman et al., 2016, 2017). The larger value $M_{MAX} = 5.5$ is also applied to estimate influence of uncertainty in maximum magnitude on the results of hazard assessment. Other parameters used in calculation (Eq. 1) are accepted as $M_{MIN} = 4.0$, $R_a = 5$ km; $d = 4$ km. Following Al-Saud (2008), earthquakes that may occur along the NNW-oriented faults are characterized by normal mechanism and earthquakes along the NE-SW trending faults—by strike-slip mechanism.

The LS model Let us consider the LS_AP variant of the linear source model (Fig. 6a), in which it is assumed that maximum magnitude earthquakes can occur along the entire length of the active faults. Distribution of the PGA values estimated using the LS_AP variant is shown in Fig. 7, and Table 1 provides the PGA estimations for selected cities Makkah and Taif. When no smoothing is applied (Fig. 7a), the zones of maximum PGAs are stretched along the faults. Three values of the smoothing operator (parameter c in Eq. 2) are considered in the smoothing procedure, namely 5 km, 7 km, and 10 km. As can be seen from Fig. 7b–d, application of the smoothing procedure does reduce the PGA estimations in the vicinity of the faults. The increase of the c value does transform the

zones of the highest PGA level from the narrow stripe-like areas along the faults (no smoothing) to the areas concentrated around the intersections of several faults (e.g., the area near the city of Makkah).

The LS_IS variant of the linear source model assumes that the maximum magnitude earthquakes can occur only in the vicinity of intersections of the active faults (see Fig. 5). As expected, the calculations performed using the LS_IS variant (Fig. 8) result (a) in concentration of the zones of the highest level of seismic hazard around intersection of the faults and (b) in reduction of the PGA values (as compared with the LS_AP variant) at relatively large distances from the intersections. The PGA values estimated for the cities of Makkah and Taif are approximately similar for the LS_AP and the LS_IS variants, because both cities are located near intersections of the active faults.

The shift of the maximum magnitude value by 0.5 unit of magnitude, i.e., from 5.0 to 5.5 does result in the increase of the corresponding PGA estimations by 1.5 times approximately. On the one hand, it shows the importance of careful estimation of maximum magnitude of possible earthquakes that can occur in the region and, on the other hand, it argues towards necessity of consideration of uncertainty in the practical calculations.

Fig. 7 Distribution of PGA (cm/s^2), LS_AP variant, M_{max} 5.0, rock site; (a) no smoothing; (b) smoothing parameter $c = 5$ km; (c) $c = 7$ km; (d) $c = 10$ km. The general linear source (LS) model is shown by black lines

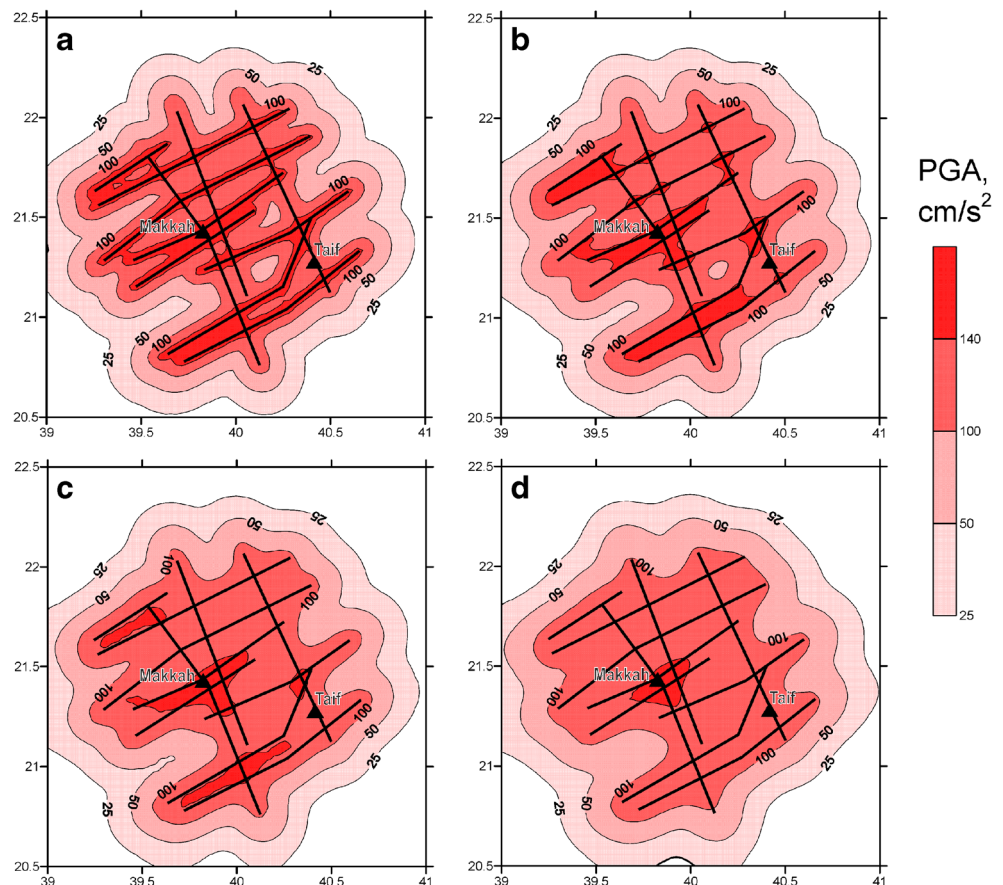


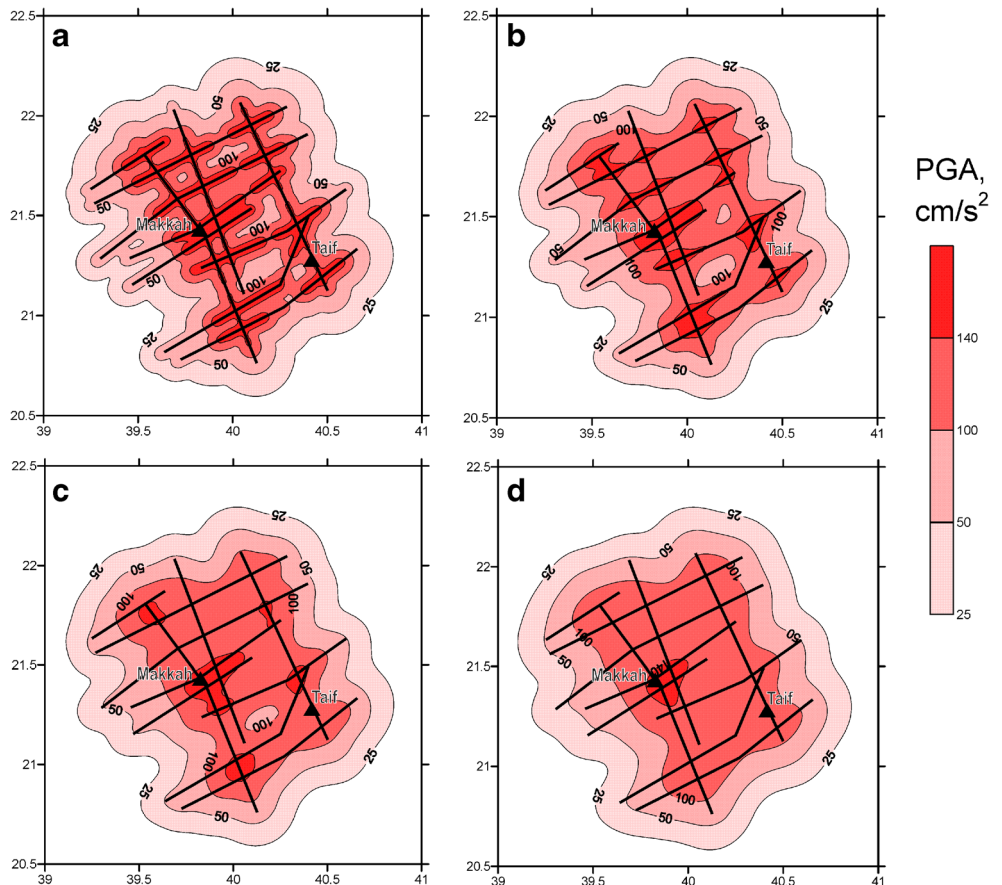
Table 1 Results of ground motion estimations (PGA cm/s^2), LS_AP model (see text) showing variations that are caused by the variations in the site condition, the maximum magnitude M_{MAX} and by application of the smoothing procedure

Site condition	GMPE value used in calculations	City		Remarks
		Makkah	Taif	
Rock	Median	155/145	140/130	Value for “no smoothing” case (Fig. 7a)/value for smoothing parameter $c = 10$ km (Fig. 7d).
	Median + 1 st. dev.	290/270	260/235	
	Dense soil	Mean	180/170	
	Median + 1 st. dev.	340/315	310/280	
Rock	Median	230/220	210/195	
	Median + 1 st. dev.	435	395	
	Dense soil	Median	265	
	Median + 1 st.dev.	490	450	

The AZ model The probability density functions and the cumulative probability functions for the rock site ($V_{s30} = 800$ m/s) PGA estimations for the cities of Makkah and Taif obtained using the AZ model are shown in Fig. 9a, b. Note that the cumulative probability is the unexceedance probability, i.e., the probability that a real-valued random variable A (PGA in this case) will take a value less than or equal to a , that is $F(a) = P(A \leq a)$.

The expected levels of ground motion from the maximum credible earthquakes may vary in a broad range depending on location of the site of interest relatively to the source zones. In our calculations, the median values, i.e., the values a for $P(A \leq a) = 0.5$, of the expected PGA are about 11.5 cm/s^2 and 7.5 cm/s^2 (rock sites) for the cities of Makkah and Taif, respectively. However, it is necessary to bear in mind that the probability functions shown in Fig. 9a, b are influenced by

Fig. 8 Distribution of PGA (cm/s^2), LS_IF variant, Mmax 5.0, rock site; (a) no smoothing; (b) smoothing parameter $c = 5$ km; (c) $c = 7$ km; (d) $c = 10$ km. The general linear source (LS) model is shown by black lines



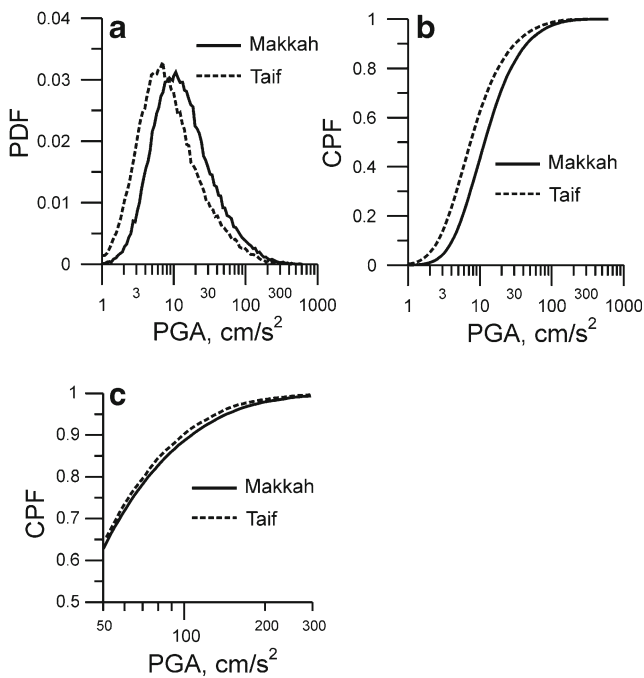


Fig. 9 Results of seismic hazard estimations using the AZ model (rock site). All data, **a** probability density functions (PDF), **b** cumulative probability functions (CPF). **c** The cumulative probability functions for PGA values above the threshold level of 25 cm/s²

numerous data from the distant events. For the goals of aseismic design and seismic risk management, it is necessary to consider influence from the events that may cause damaging level of ground motion. Therefore, as suggested by Sokolov (2017), for analysis of the data from numerous scenario earthquakes, it seems to be useful considering distribution of the ground motion values *A* above the certain threshold level *A*₀. The description of the technique taken from Sokolov (2017) is provided below.

Cumulative distribution function, that is unexceedance, for the random values *a* above the threshold level *A*₀ is denoted as $F_{A_0}(a) = P(A \leq a | A_0)$; the function varies from 0 for *a* = *A*₀ to ~ 1 at sufficiently large *a* values. Let us assume that macroseismic intensity may be used as a simple characteristic of earthquake damage. Sokolov (2017) suggested considering the relationship between macroseismic intensity and ground motion parameter for selection of the threshold level *A*₀. In terms of the Modified Mercalli (MM) scale, macroseismic intensity MM V characterizes the highest level of ground motion (moderate shaking), under which the damage to ordinary buildings would not occur or may be considered as negligible. Thus, the threshold level may be accepted as the level of ground motion that corresponds to the intensity MM V, that is *A*_{MM V}. The higher the level of ground motion exceeding the threshold level, the larger degree of expected damage.

Sokolov (2017) provided several PGA values that, in average, correspond to the intensity MM V (*PGA*_{MM V}), as follows. The *PGA*_{MM V} was estimated by Chernov (1989) as

25 cm/s² using the worldwide database. Worden et al. (2012) obtained *PGA*_{MM V} = 60 cm/s² for the Californian earthquakes; this relatively high value does reflect advanced seismic design standards in the region. Bilal and Askan (2014) analyzed the Turkish data based on the building stock mostly not complying with the current seismic regulations and their MMI-PGA relation resulted in *PGA*_{MM V} of about 15 cm/s². In our study, we use the threshold value of 25 cm/s² and the results of the corresponding assessments for the cities of Makkah and Taif are shown in Fig. 9c and listed in Table 2. As can be seen from the Tables 1 and 2, the estimation obtained using the LS models and considering the median GMPE values roughly correspond to the AZ estimations for $P(A \leq a | 25 \text{ cm/s}^2) = 0.95$.

Figure 10 shows distribution of PGA values estimated for probability of unexceedance $P(A \leq a | 25 \text{ cm/s}^2) = 0.95$ that allows direct comparison of the map with those constructed using the LS models (Figs. 7 and 8). The highest PGA values in the AZ estimations are concentrated around intersections of faults that implicitly considers high probability of earthquake occurrence in these areas. Note, that the AZ estimations are obtained without application of the smoothing procedure as that when using the LS models. At the same time, the level of hazard (PGA values) estimated using the AZ model for relatively large distances from the seismic sources (e.g., near the borders of considered region) is much higher than that estimated using the LS model. The phenomenon reflects consideration of ground motion variability in the calculations performed using the AZ model.

Discussion

It is useful, both from the methodological and the practical points of view, to compare the results of seismic hazard assessment obtained using the LS and the AZ models.

Table 2 Results of hazard assessments, AZ model, PGA estimations for different probabilities of unexceedance $P(A \leq a | A_{MM V})$, *A*_{MM V} = 25 cm/s². Values in parentheses show ranges of estimation obtained using the LS model (see Table 1)

City	Probability of unexceedance $P(A \leq a 25 \text{ cm/s}^2)$			
	0.8	0.9	0.95*	0.99**
Rock				
Makkah	75	105	145 (155–145)	255 (290–270)
Taif	70	100	130 (140–130)	230 (260–235)
Dense soil				
Makkah	78	115	160 (180–170)	290 (340–315)
Taif	75	105	145 (165–155)	250 (310–280)

*Median GMPE in the LS model

**Median + 1 st. dev. in the LS model

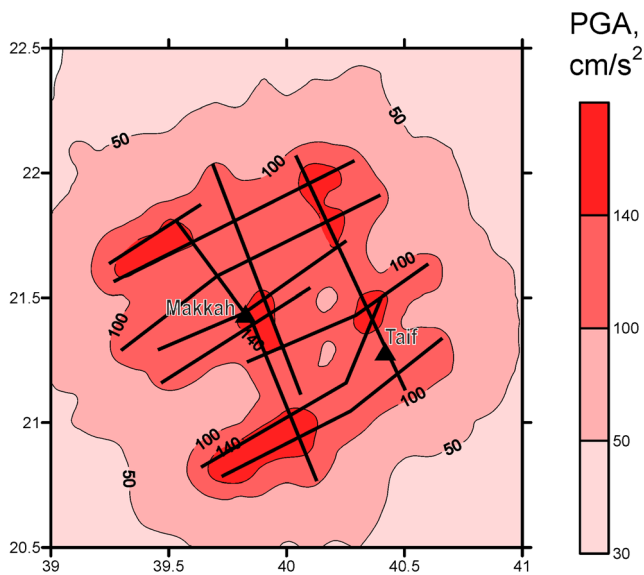


Fig. 10 Distribution of PGA (cm/s^2), AZ model, Mmax 5.0, rock site; PGA estimations obtained for probability of unexceedance $P(A \leq a | 25 \text{ cm/s}^2) = 0.95$. The general linear source (LS) model of active faults is shown by black lines

Application of the LS model implicitly considers the highest level (or, strictly speaking, the level that is close to maximum) of possible ground motion expected from the closest maximum magnitude earthquake. Thus, when the probability functions in the AZ variant of calculations are constructed using all data (Fig. 9a, b), the estimations obtained using the LS model, even for the median GMPE, correspond to very high probabilities of unexceedance (e.g., $P(A \leq a) > 0.99 - 0.995$) in the AZ variant. When considering the probability functions for the ground motion values above the threshold level of 25 cm/s^2 (or MMI V), the estimations obtained using the LS model relate to those obtained using the AZ model as follows (see Tables 1 and 2): $P(A \leq a | 25 \text{ cm/s}^2) \sim 0.95$ for the median GMPE used in the LS calculations, and $P(A \leq a | 25 \text{ cm/s}^2) \geq 0.99$ for the median GMPE +1 st. dev. used in the LS calculations.

Sokolov (2017) suggested using a special term for the value of ground motion a above threshold level that may be exceeded with particular probability. Let us assume that the design level a_D was selected for particular probability of unexceedance $P(A \leq a | A_{MMV})$, say 90%. It means that if numerous maximum credible earthquakes will occur around the site of interest, the intensity of ground shaking causing damage (MMI > V) will be larger than the selected design level a_D during only 10% of the total number of the earthquakes. Thus, the value a_D may be called as “ N %-safety” ground motion parameter, where N denotes the probability of exceedance $P(A \leq a | A_{MMV})$ expressed as percentage, or “90%-safety” in the considered case. The term describes in qualitative manner the relation between the design ground motion and the degree of expected damage, as follows: the

Table 3 Comparison of deterministic seismic hazard estimation for the city of Makkah

Source	PGA cm/s^2	Remarks
Our study (Table 1)	145–155	Median GMPE
	270–290	Median + 1 st. dev. GMPE
Rehman et al. (2016)	110–120	Median PGA results
	200	84% fractile PGA results
Osman (2012)	80	Median GMPE, MCE 4.8

higher design ground motion (above 25 cm/s^2), the lower level of expected damage, and the higher safety of construction. Thus, the estimations of seismic hazard based on the AZ model allow flexible selection of design ground motion considering the level of safety (e.g., 90%, 95%, or 99%) and correspondingly the importance of construction.

Alternatively, the term “ N %-damage” may be used when considering complimentary cumulative distribution function or probability of exceedance $P(A > a | A_{MMV})$, that is “10%-damage” in the considered case. Again, the term does not describe in quantitative manner the expected degree of damage for particular structures subjected by given level of ground motion A . The degree of damage has to be estimated using construction-specific fragility functions for given level of ground motion.

Several estimations of seismic hazard were performed recently for the Makkah area using different approaches and input data and models (Table 3). Apparently, the DSHA estimations for the city of Makkah obtained in our work are higher than those reported by other researches. Most likely, the discrepancy, besides the smaller maximum magnitude value used by Osman (2012), is caused by different ground motion prediction equations applied in the studies, as well as by different techniques of calculations. The discrepancy reflects epistemic (or modeling) uncertainty that is related to input data, used models and techniques, and that is the dominate source of uncertainty in natural hazard assessment (e.g., Beven et al. 2015). The results obtained by different methods describe seismic hazard from different points of view and, therefore, they provide a basis for judgment about reliability and uncertainty of the hazard maps.

Conclusion

In this work, we apply deterministic seismic hazard assessment to evaluate level of seismic hazard in terms of peak ground acceleration (PGA) for the Makkah region. Different techniques are used for the assessment; presumably, active geological faults are considered as the sources of earthquakes. Results of the study show that, in the context of the used models of seismic sources, the level of seismic hazard in the

region is controlled by magnitude of earthquakes that may occur at the intersection of NE-SW faults (the Ad Damm fault zone and the Wadi Fatima Shear Zone) and the NNW-oriented faults that run parallel to the Red Sea coast (Red Sea Margin Faults group). Thus, it is important to make accurate mapping of the faults using geological, geophysical, and seismological data, and to estimate if the faults are active at present. On the other hand, particular attention should be given to careful estimation of the maximum magnitude of possible earthquakes that can occur along the active fault. Comprehensive consideration of uncertainties in characteristics of earthquake sources and in seismic wave propagation should be included in the seismic hazard study.

Bearing in mind that the deterministic seismic hazard analysis is used for design of important and critical infrastructures, and emergency response and recovery, the results of this study may be useful to constrain the expected level of maximum ground motion in the region. However, the models of seismic sources used in this study do not take into account the earthquakes that may occur outside the considered region. Therefore, the level of seismic hazard estimated at relatively large distances from the considered active faults (i.e., near the borders of the region) may be underestimated.

Acknowledgments The authors are grateful to Prof. Abdullah Al-Amri for the seismic data obtained before 2000 and to anonymous reviewer for the thorough comments. The work has been performed in the National Center for Earthquakes and Volcanoes, Saudi Geological Survey, Jeddah, Kingdom of Saudi Arabia.

References

- Abdelfattah AK, Morgen S, Mukhopahyay M (2016) Mapping b-value for 2009 Harrat Lunayyir earthquake swarm, western Saudi Arabia and Coulomb stress for its mainshock. *J Volcanol Geotherm Res* 330:14–23
- Akkar S, Sandikkaya MA, Bommer JJ (2014) Empirical ground-motion models for point- and extended-source crustal earthquake scenarios in Europe and the Middle East. *Bull Earthq Eng* 12(1):359–387
- Al-Amri AM (1995) Recent seismic activity in the northern Red Sea. *Geodynamics* 20:243–253
- Al-Saud MM (2008) Seismic characteristics and kinematic models of Makkah and Central Red Sea regions. *Arab J Geosci* 1:49–61. <https://doi.org/10.1007/s12517-008-0004-2>
- Ambraseys NN, Adams RD (1988) The seismicity of Saudi Arabia and adjacent areas: part B. Department of Civil Engineering, Imperial College of Science and Technology, London ICST/KACST Project, ESEE Rep. no. 88/11
- Ambraseys NN, Melville CP (1988) The seismicity of Saudi Arabia and adjacent areas: part A. Department of Civil Engineering, Imperial College of Science and Technology, London ICST/KACST Project, ESEE Rep. no. 88/11
- Ambraseys NN, Melville CP, Adams RD (1994) The seismicity of Egypt, Arabia and the Red Sea: a historical review. Cambridge University Press, Great Britain 181 pp
- Atkinson GM, Boore DM (2006) Earthquake ground-motion prediction equations for Eastern North America. *Bull Seismol Soc Am* 96: 2181–2205
- Babiker N, Mula AHG, El-Hadidy S (2015) A unified Mw-based earthquake catalogue and seismic source zones for the Red Sea region. *J Afr Earth Sci* 109:168–176. <https://doi.org/10.1016/j.jafrearsci.2015.05.011>
- Baer G, Hamiel Y (2010) Form and growth of an embryonic continental rift: InSAR observations and modelling of the 2009 western Arabia rifting episode. *Geophys J Int* 182:155–167
- Beven KJ, Aspinall WP, Bates PD, Borgomeo E, Goda K, Hall JW, Page T, Phillips JS, Rougier JT, Simpson M, Stephenson DB, Smith PJ, Wagener T, Watson M (2015) Epistemic uncertainties and natural hazard risk assessment – part 1: a review of the issues. *Nat Hazards Earth Syst Sci Discuss* 3:7333–7377. <https://doi.org/10.5194/nhessd-3-7333-2015>
- Bilal M, Askan A (2014) Relationships between felt intensity and recorded ground-motion parameters for Turkey. *Bull Seismol Soc Am* 104: 484–496. <https://doi.org/10.1785/0120130093>
- Blank HR (1977) Aeromagnetic and geological study of tertiary dikes and related structures on the Arabian margin of the Red Sea. In: Saudi Arabian Directorate General of Mineral Resources. Red Sea Research 1970–1975, Bulletin no. 22, G1–18
- Boore DM, Atkinson GM (2008) Ground-motion prediction equations for the average horizontal component of PGA, PGV, and 5%-damped PSA at spectral periods between 0.01 s and 10.0 s. *Earthquake Spectra* 24:99–138
- Bosworth W (2015) Geological evolution of the Red Sea: historical background, review, and synthesis. In: Rasul NMA, Stewart ICF (eds) *The Red Sea*. Springer Earth System Sciences, Berlin Heidelberg, pp 45–78. https://doi.org/10.1007/978-3-662-45201-1_3
- Camp VE, Roobol MJ (1989) The Arabian continental alkali basalt province: part I. Evolution of Harrat Rahat, Kingdom of Saudi Arabia. *Bull Geol Soc Am* 101:71–95
- Camp VE, Roobol MJ (1992) Upwelling asthenosphere beneath western Arabia and its regional implications. *J Geophys Res* 97:15255–15271
- Camp VE, Hooper PR, Roobol MJ, White DL (1987) The Madinah eruption, Saudi Arabia: Magma mixing and simultaneous extrusion of three basaltic chemical types. *Bull Volcanol* 49:489–508. <https://doi.org/10.1007/BF01245475>
- Camp VE, Roobol MJ, Hooper PR (1991) The Arabian continental alkali basalt province: part II. Evolution of Harrat Khaybar, Ithnayn, and Kura, Kingdom of Saudi Arabia. *Bull Geol Soc Am* 103:363–391
- Campbell KW, Bozorgnia Y (2008) NGA ground motion model for the geometric mean horizontal component of PGA, PGV, PGD and 5%-damped linear elastic response spectra at periods ranging from 0.1 s to 10.0 s. *Earthquake Spectra* 24:139–171
- Chernov YK (1989) Strong ground motion and quantitative assessment of seismic hazard. Fan Publishing House, Tashkent (in Russian)
- Deif A, Zahran HM, El-Hadidy MS, Bawajeeh AO, El-Hadidy SY, Mansoub TA (2009) Seismic hazard assessment along Haramain high speed rail project (Makkah-Madinah). Saudi Geological Survey report, 150 pp
- Downs DT, Stelten ME, Champion DE, Dietterich HR, Nawab Z, Zharan H, Hassan K, Shawali J (2018) Volcanic history of the northernmost part of the Harrat Rahat volcanic field, Saudi Arabia. *Geosphere* 14(3):1253–1282. <https://doi.org/10.1130/GES01625.1>
- Duncan RA, Al-Amri AM (2013) Timing and composition of volcanic activity at Harrat Lunayyir, western Saudi Arabia. *J Volcanol Geotherm Res* 260:103–116
- El-Hadidy SY (2015) Seismicity and seismotectonic setting of the Red Sea and adjacent areas. In: Rasul NMA, Stewart ICF (eds) *The Red Sea*. Springer Earth System Sciences, Berlin Heidelberg, pp 151–159. https://doi.org/10.1007/978-3-662-45201-1_8
- El-Hadidy SY, Zahran HM, El-Hadidy M, Sami M (2015) Seismicity and seismotectonic settings of western Saudi Arabia with special emphasis of 5.1 Baish-Jizan earthquake 2014. Workshop on Imaging and Active Tectonics of the Red Sea Region. King Abdulaziz University

- of Science and Technology (KAUST), Kingdom of Saudi Arabia, March 10–13, 2015
- El-Isa ZH, Al Shanti A (1989) Seismicity and tectonics of the Red Sea and western Arabia. *Geophys J* 97:449–457
- El-Masry NN, Moufti MRH, Nemet K, Murcia H, Qaddah AA, Abdelwahed MF (2013) Historical accounts of the AD 1256 eruption near Al-Madinah. In: Proceedings of the VORISA scientific meeting, 17–18 November 2013. King Abdulaziz University, Jeddah, p. 9–13
- Endo E, Zahran H, Nofal H, Hadidy S (2007) The Saudi National Seismic Network. *Seismol Res Lett* 78:439–445. <https://doi.org/10.1785/gssrl.78.4.439>
- Fnais MS, Abdelrahman K, El-Hady Sh, Abdel-Monem E (2014) Seismicity and seismotectonics of the Jeddah area, Saudi Arabia. *WIT Trans State Art Sci Eng* 79. <https://doi.org/10.2495/978-1-84564-978-4/01>
- Girdler RW (1991) The Afro-Arabian rift system – an overview. *Tectonophysics* 197:139–153
- Johnson PR (1998) Tectonic map of Saudi Arabia and adjacent areas. Ministry of Petroleum and Mineral Resources, Deputy Ministry for Mineral Resources, Technical Report USGS TR-98-3 (IR 948)
- Kassem OMK, Hamimi Z (2018) Finite strain analysis of the Wadi Fatima Shear Zone in Western Arabia, Saudi Arabia. *Geotectonics* 52(2):251–265. <https://doi.org/10.1134/S0016852118020036>
- Klügel J-U (2008) Seismic hazard analysis - quo Vadis. *Earth-Sci Rev* 88: 1–32
- Klügel J-U, Mualchin L, Panza GF (2006) A scenario-based procedure for seismic risk analysis. *Eng Geol* 88:1–22
- McGuire RK (2001) Deterministic vs. probabilistic earthquake hazard and risks. *Soil Dyn Earthq Eng* 21:377–384
- Merghealani HM, Kinkar AR, As-Sawwaf MW (1981) Seismicity studies in Saudi Arabia-Microearthquakes in the Jiddah area: Saudi Arabian Directorate General of Mineral Resources Open-File Report DGMROF-01-08, 64 p
- Moore TA, Al-Rehaili MH (1989) Explanatory notes to the geologic map of the Makkah quadrangle, sheet 21D, Kingdom of Saudi Arabia. Ministry of Petroleum and Mineral Resources, 62 p
- Moufti MR, Németh K, Murcia H, Lindsay JM (2013) The 1256 AD Al Madinah historic eruption geosite as the youngest volcanic chain in the Kingdom of Saudi Arabia. *Int J Earth Sci* 102(4):1069–1070
- Mukhopadhyay B, Mogren S, Mukhopadhyay M, Dasgupta S (2013) Incipient status of dyke intrusion in top crust – evidences from the Al-Ays 2009 earthquake swarm, Harrat Lunayyir, SW Saudi Arabia. *Geomat. Nat Hazards Risk* 4(1):30–48
- Osman A (2012) Seismic hazard analysis and development of ground motion parameters for Makkah region in Saudi Arabia. In: proceedings of the 15th World Conference on Earthquake Engineering, Lisbon, Portugal, 24–28 September 2012, http://www.iitk.ac.in/nicee/wcee/article/WCEE2012_2736.pdf. Accessed 5 Feb 2019
- Pallister JS (1986) Explanatory notes to the geologic map of the Al Lith quadrangle, sheet 20D, Kingdom of Saudi Arabia. Ministry of Petroleum and Mineral Resources, 41 p
- Pallister JS, McCausland WA, Jónsson S, Lu Z, Zahran HM, El Hadidy S, Aburukbah A, Stewart ICF, Lundgren PR, White RA, Moufti MRH (2010) Broad accommodation of rift-related extension recorded by dike intrusion in Saudi Arabia. *Nat Geosci* 3:705–712
- Panza GF (2017) NDSHA: robust and reliable seismic hazard assessment. Proceedings, International Conference on Disaster Risk Mitigation, Dhaka, Bangladesh, September 23–24, 2017, arXiv:1709.02945
- Panza GF, Peresan A, La Mura C (2013) Seismic hazard and strong ground motion: an operational neodeterministic approach from national to local scale. *Geophysics and Geochemistry*. In: UNESCOEOLSS Joint Committee (eds) *Encyclopedia of life support systems (EOLSS)*, developed under the Auspices of the UNESCO. Eolss Publishers, Oxford. <https://www.eolss.net/Sample-Chapters/C01/E6-16-52.pdf>. Accessed 21 July 2019
- Panza GF, Kossobokov VG, Peresan A, Nekrasova A (2014) Why are the standard probabilistic methods of estimating seismic hazard and risk too often wrong. In: Wyss M (ed) *Earthquake hazard, risk and disasters*. Elsevier, Waltham, pp 309–357. <https://doi.org/10.1016/B978-0-12-394848-9.00012-2>
- Poirier JP, Taher MA (1980) Historical seismicity in the near and Middle East, North Africa and Spain from Arabic documents (VIIth–XVIIIth century). *Bull Seismol Soc Am* 70:2185–2201
- Rehman F, El-Hady SM, Atef AH, Harbi HM (2016) Seismic hazard assessment of Western Coastal Province of Saudi Arabia: deterministic approach. *Earthq Sci* 29(5):299–309. <https://doi.org/10.1007/s11589-016-0164-1>
- Rehman F, Alamri AM, El-Hady HHM, Atef AH (2017) Seismic hazard assessment and rheological implications; a case study selected for cities of Saudi Arabia along the eastern coast of Red Sea. *Arab J Geosci* 10:540. <https://doi.org/10.1007/s12517-017-3325-1>
- Roobol MJ, Kadi KA (2008) Cenozoic faulting in the Rabigh area, central west Saudi Arabia (including the sites of King Abdullah Economic City and King Abdullah University for Science and Technology). Saudi Geological Survey Technical Report SGS-TR-2008-6, 1:250, 000 map, with text 12 p
- Roobol MJ, Kadi KA (2014) Cenozoic faulting in the Jizan area, Southwest Saudi Arabia. Saudi Geological Survey Technical Report SGS-TR-2013-14, 32 p., 18 figs, 3 plates
- Roobol MJ, Stewart ICF (2009) Cenozoic faults and recent seismicity in Northwest Saudi Arabia and the Gulf of Aqaba region. Saudi Geological Survey Technical Report SGS-TR-2008-7, 35 p., 35 figs, 2 app., 10 plates
- Saudi Building Code SBC-301-2007. Loads and Forces Requirements. Saudi Building Code National Committee
- Sokolov V (2017) Seismic hazard analysis based on maximum credible earthquakes. *Bull Earthq Eng* 15(5):1831–1852. <https://doi.org/10.1007/s10518-016-0059-5>
- Sokolov V, Zahran HM (2018) Seismic hazard analysis for development of risk-targeted ground-motion maps in the western Saudi Arabia, Proceedings 16-th European Conference on Earthquake Engineering, 18–21 June 2018, Thessaloniki, Greece, paper 10424
- Sokolov V, Zahran HM, El-Hadidy SY, El-Hadidy M, Alraddi WW (2017) Seismic hazard assessment for Saudi Arabia using spatially smoothed seismicity and analysis of hazard uncertainty. *Bull Earthq Eng* 15:2695–2735. <https://doi.org/10.1007/s10518-016-0075-5>
- Stern RJ, Johnson PR (2010) Continental lithosphere of the Arabian plate: a geologic, petrologic, and geophysical synthesis. *Earth-Sci Rev* 101:29–67. <https://doi.org/10.1016/j.jears.2010.01.002>
- Stewart ICF, Miller DT (2018) Directional tilt derivatives to enhance structural trends in aeromagnetic grids. *J Appl Geophys* 159:553–563. <https://doi.org/10.1016/j.jappgeo.2018.10.004>
- Thenhaus PC, Algermissen ST, Perkins DM, Hanson SL, Diment WH (1989) Probabilistic estimates of the seismic ground-motion hazard in Western Saudi Arabia. *US Geological Survey Bull* 1868, 42 p
- Vakov AV (1996) Relationships between earthquake magnitude, source geometry and slip mechanism. *Tectonophysics* 261:97–113
- Whiteman AJ (1976) The existence of transform faults in the Red Sea depression. *Philos Trans R Soc Lond A* 267:407–408
- Worden CB, Gerstenberger MC, Rhoades DA, Wald DJ (2012) Probabilistic relationships between ground motion parameters and modified Mercalli intensity in California. *Bull Seismol Soc Am* 102: 204–221. <https://doi.org/10.1785/0120110156>
- Zahran HM, El-Hady SM (2017) Seismic hazard assessment for Harrat Lunayyir – a lava field in western Saudi Arabia. *Soil Dyn Earthq Eng* 200:428–444
- Zahran HM, Stewart ICF, Johnson PR, Basahel MH (2003) Aeromagnetic-anomaly maps of central and western Saudi Arabia. Saudi Geological Survey Open-File Report SGS-OF-2002-8, 6 p., 1 fig, 1 table, 4 sheets (scale 1:2,000,000)

- Zahran HM, Sokolov V, El-Hadidy S, Alraddi WW (2015) Preliminary probabilistic seismic hazard assessment for the Kingdom of Saudi Arabia based on combined areal source model: Monte Carlo approach and sensitivity analyses. *Soil Dyn Earthq Eng* 77:453–468. <https://doi.org/10.1016/j.soildyn.2015.06.011>
- Zahran HM, Sokolov V, Roobol MJ, Stewart ICF, El-Hadidy S, El-Hadidy M (2016) On the development of a seismic source zonation model for seismic hazard assessment in western Saudi Arabia. *J Seismol* 20(3): 747–769. <https://doi.org/10.1007/s10950-016-9555-y>
- Zahran HM, El-Hady SM, Abuelnaga HS (2017) Aeromagnetic data over Harrat Lunayyir and surrounding areas, western Saudi Arabia. *Arab J Geosci* 10:63. <https://doi.org/10.1007/s12517-017-2849-8>
- Zhao JX, Zhang J, Asano A, Ohno Y, Oouchi T, Takahashi T, Ogawa H, Irikura K, Thio HK, Somerville PG, Fukushima Y (2006) Attenuation relations of strong ground motion in Japan using site classifications based on predominant period. *Bull Seismol Soc Am* 96:898–913
- Zuccolo E, Vaccari F, Peresan A, Panza GF (2011) Neo-deterministic and probabilistic seismic hazard assessments: a comparison over the Italian territory. *Pure Appl Geophys* 168:69–83. <https://doi.org/10.1007/s00024-010-0151-8>